NMR Signature of Evolution of Ductile-to-Brittle Transition in Bulk Metallic Glasses

C. C. Yuan,[1] J. F. Xiang,[2] X. K. Xi,[1,*] and W. H. Wang[1]
[1]Institute of Physics, Chinese Academy of Sciences, Beijing, 100190, China
[2]Institute of Chemistry, Chinese Academy of Sciences, Beijing, 100190, China
(Received 25 June 2011; published 30 November 2011)

The mechanical properties of monolithic metallic glasses depend on the structures at atomic or subnanometer scales, while a clear correlation between mechanical behavior and structures has not been well established in such amorphous materials. In this work, we find a clear correlation of ^{27}Al NMR isotropic shifts with a microalloying induced ductile-to-brittle transition at ambient temperature in bulk metallic glasses, which indicates that the ^{27}Al NMR isotropic shift can be regarded as a structural signature to characterize plasticity for this metallic glass system. The study provides a compelling approach for investigating and understanding the mechanical properties of metallic glasses from the point of view of electronic structure.

DOI: 10.1103/PhysRevLett.107.236403 PACS numbers: 71.23.Cq, 76.60.−k, 81.40.Lm

A detailed description of atomic structure and bonding characteristics underpins our understanding of condensed solids. In particular, it has been long suggested that monolithic metallic glasses (MGs) can be distinguished from their bonding states and structural characteristics in short and/or medium range order [1,2]. Classical structural models such as free volume [3] or shear transformation zone (STZ) [4], and dense random packing [5] or efficient cluster packing [6,7] theories have been used to describe plastic flow and fracture nicely, whereas those models in terms of packing based on atomic size and configuration (local topology and symmetry [8]) fails to take consideration of the details of the nature of atomic bonding in MGs, which is indispensable for a better understanding of their mechanical behavior. Recently, theoretical calculations illuminated that the hybrid character of interatomic bond of multicompositions contribute to the elastic properties [9], and bond flexibility or mobility might determine intrinsic plasticity versus brittleness properties [10,11]. Nevertheless, the order parameter(s) which can be accessed by experiments to characterize the nature of bond mobility and its evolution upon alloying in MGs is still lacking. The evolution of local bonding in MGs could have consequences on experiments that are sensitive to local susceptibility of electronic states, such as NMR [12]. In contrast to conventional approaches such as specific heat and magnetic susceptibility experiments, NMR allows one to selectively probe the local electronic band structure change on certain atomic sites induced by alloying [13]. ^{27}Al NMR has been proved to be an excellent atomic probe for effective structural analyses of local bonding of Al atoms in a transition-metal matrix [14–16]. As an solute atom surrounded by transition-metal (TM) atoms in MGs, Al makes up of Al-centered clusters which is proposed to play a key role on plastic flow involved in stress-induced cooperative rearrangement [17]. The hybridization of Al $3p$ with TM d states in MGs strongly resists Al-TM bond mobility [18,19], and hence shearing strain. Since shear stress required for activating the STZ scales with the shear modulus [20], electronic structure changes which affect the shear modulus should have a pronounced effect on the mechanical properties.

In this letter, ^{27}Al NMR spectroscopy was employed as an atomic probe to investigate the evolution of bonding states for composition induced brittle-to-ductile transition (BDT) in a model $ZrCuNiAlSn_x$ MG system under ambient condition. We report a ^{27}Al NMR signature to characterize the bonding states during BDT in the model MG. Our results show that the plasticity vs brittleness properties of MGs can be understood on a fundamental level in terms of their distinct bonding nature. The study provides a compelling approach to distinguish MGs from an electronic structural point of view, as a complementary to the common views focused on atomic configuration.

The amorphous nature of the $Zr_{61}Cu_{18.3-x}Ni_{12.8}Al_{7.9}Sn_x$ ($0 \leq x \leq 2.5$) glassy samples was ascertained by x-ray diffraction and differential scanning calorimetry. Structural analyses were performed by using two independent ^{27}Al nuclear magnetic resonance (NMR) experiments [21]: (1) composition dependence using Bruker AVANCE^{TM} III with a magnetic field of 9.39 T at 298 K; (2) field and temperature dependence using an Oxford magnet with magnetic fields tunable from 3.6 to 10.3 T and temperatures from 5 to 80 K. rf field strength and ^{27}Al shift were calibrated with references, 1M $Al(NO_3)_3$ solution in experiment (1) and Cu wire in (2). All ^{27}Al NMR time domain signals were recorded using Hahn echo sequences and then Fourier transformation was performed. The selected pulse durations were carefully selected and short enough to avoid the distortion of the central lines associated with the central transition ($m = -1/2 \leftrightarrow +1/2$). The first pulse duration is 3 μs in experiment (1); while it is 8 μs in experiment (2).

The mechanical properties of ZrCuNiAl MGs can be tuned by tiny addition of tin. Figure 1 plots prenotch fracture toughness (K_Q), compressive plastic strain (ε_p), and plastic process zone size (w) versus the concentration of Sn for $ZrCuNiAlSn_x$. The fracture toughness undergoes an obvious BDT, reaches its maximum 46.2 MPa $m^{1/2}$ at 1 at. % Sn and decreases to 16.3 MPa $m^{1/2}$ with 2.5 at. % Sn alloying. The compressive plastic strain, ε_p exhibits a similar sharp transition as increasing Sn concentration. ε_p significantly drops from 11% to near zero with a corresponding concentration of Sn from 1.5% to 2.5%. Scanning electron microscope images on top of Fig. 1 show the evolution of fracture morphology of bending samples with the concentration of Sn: 1, 2 and 2.5 at. % at the dominant Mode I crack surface regions. The characteristic dimplelike patterns on fracture surfaces nonmonotonically varies with Sn concentration, displaying a compositional dependence of BDT as well. Therefore, $ZrCuNiAlSn_x$ is chosen as a model system in our studies owing to the significant variety of mechanical behaviors with minute composition change.

Figure 2(a) shows central line shape of powder spectra of $Zr_{61}Cu_{18.3-x}Ni_{12.8}Al_{7.9}Sn_x$ MGs with $x = 0$, 0.5 and 2.5, measured at 298 K. The isotropic Knight shift was determined by the peak position of the central transition. Isotropic Knight shift (K_{iso}) of sp element such as Al has been correlated with electronic structure and bonding character in MGs. Since the orbital *Van Vleck* contribution to K_{iso} for sp element Al is usually small and it nearly cancels with the diamagnetic term. For simplicity, excluding the smaller contributions of orbital paramagnetism, core polarization contributed from d states at the Fermi energy, ^{27}Al NMR isotropic shifts in weakly paramagnetic or nonmagnetic Al-containing MGs are predominantly

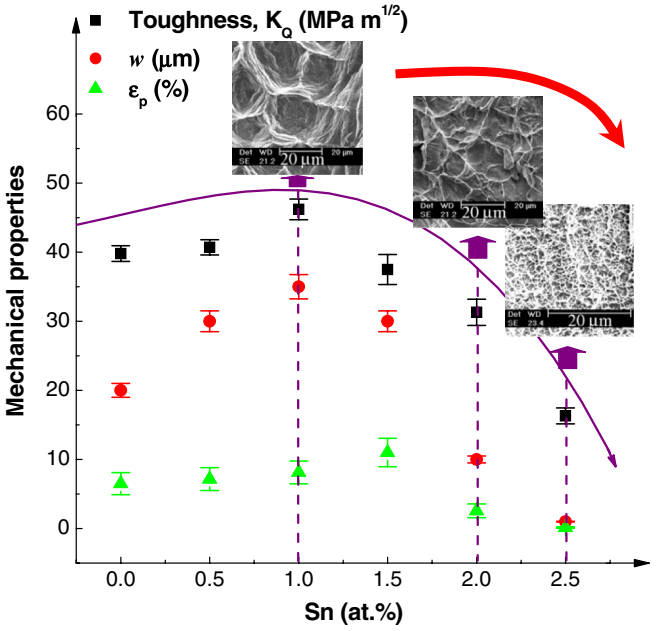

FIG. 1 (color online). Characterization of brittle-to-plastic transition in $Zr_{61}Cu_{18.3-x}Ni_{12.8}Al_{7.9}Sn_x$ MGs with $0 \leq x \leq 2.5$. Black squares represent prenotched toughness; red circles represent plastic process zone size; green triangles represent plastic strain; The inset displays the evolution of fracture morphology as a function of Sn concentration.

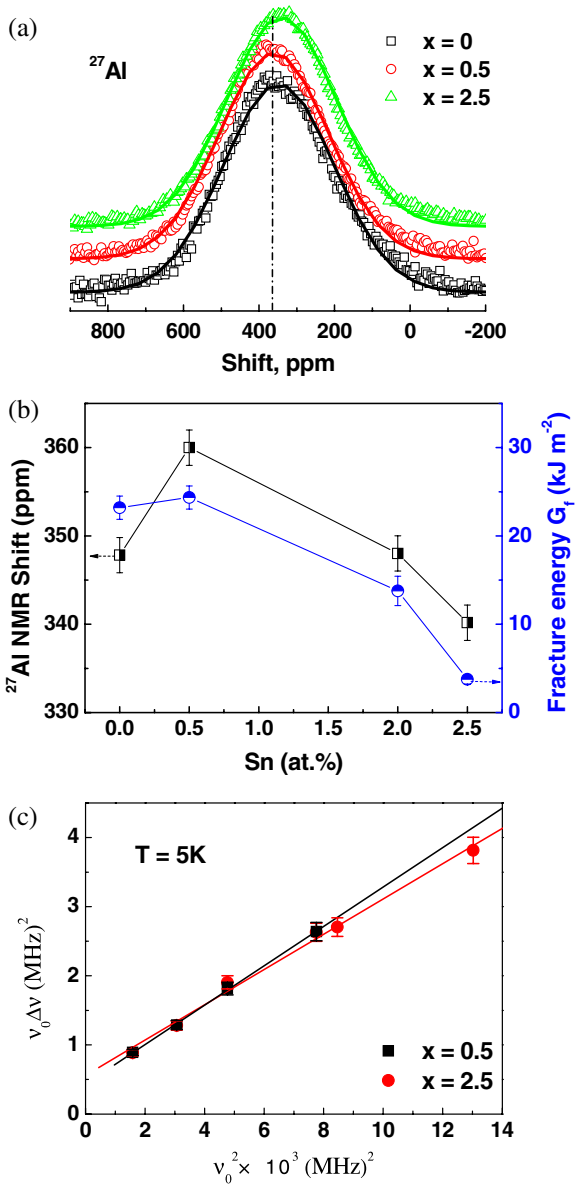

FIG. 2 (color online). (a) Representative ^{27}Al NMR central line shape of powder spectra of $Zr_{61}Cu_{18.3-x}Ni_{12.8}Al_{7.9}Sn_x$ MGs with $x = 0$, 0.5 and 2.5. The ^{27}Al NMR spectra are normalized to the maximum intensity for various Sn concentrations and taken at $H = 9.39$ Tesla and $T = 298$ K. The solid lines are fitted with Gaussian distribution. (b) The correlation of ^{27}Al NMR line shift (left coordinate) and fracture energy (right coordinate) with Sn concentration; The solid lines and arrows are for guiding eyes. (c) Frequency dependence of the ^{27}Al line width. The solid line is a fitting by the form $\nu_0\Delta\nu = a + b\nu_0{}^{\wedge 2}$.

direct contact shifts reflecting the magnetic coupling of nucleus to the s character of conduction electrons [13]:

$$K = \frac{16\pi}{3}\mu_B^2\langle|\psi(0)|^2\rangle_{E_F} g_s(E_F),$$

where, μ_B is the Bohr magneton, $\langle|\Psi(0)|^2\rangle$ is the average probability density at the nucleus for electronic states on the Fermi surface and $g_s(E_f)$, s density of states at the Fermi level. The evolution of bonding characters will be manifested as the response of isotropic Knight shifts [13–15].

Significant changes of Knight shifts as a function of Sn concentration can be seen in Fig. 2(b). This observation strongly suggests these MGs can be distinguished from each other by $g_s(E_f)$ or bonding states on Al sites. Figure 2(b) also shows the relationship of ^{27}Al Knight shifts with fracture energy. Under the plane strain state, $G_f = {K_Q}^2/E(1-\nu^2) \approx 2\gamma_s + \gamma_p$, where ν is the Poisson's ratio, and G_f is employed to evaluate the energy dissipation on fracture process, including surface energy, γ_s, and plastic work energy, γ_p. The term, γ_s, usually about $\gamma_p/1000$ for quasibrittle materials [22], can be neglected. Thus, G_f is approximately γ_p, as a parameter reflecting local plastic deformation ability at the crack tip. It can be seen Knight shifts and fracture energy both have a similar change tendency upon the variation of Sn concentration, and show the maximum peak around the composition with 0.5% Sn. The samples show the largest fracture energy of 23.2 kJ m^{-2} with 0.5% Sn having the largest shift of 360 ppm among these MGs, then drop to 3.8 kJ m^{-2} with 2.5% Sn associated with the obvious decrease of the ^{27}Al shift. The similar variation tendency of fracture energy and ^{27}Al Knight shifts upon the change of Sn content reveals that the plasticity of MGs are well correlated with the bonding characters revealed by ^{27}Al shifts.

^{27}Al shifts and line width (full width at half magnitude, $\Delta\nu$) at variable fields were examined for Sn = 0.5 and 2.5 at. % samples. ^{27}Al shifts exhibit field and temperature independence. However, $\Delta\nu$ shows to be strongly nonlinearly dependent on Larmor frequency (ν_0). As shown in Fig. 2(c), $\Delta\nu$ can be fitted perfectly with the equation $\nu_0\Delta\nu = a + b{\nu_0}^{\wedge 2}$, where $a = (25/18){\nu_Q}^{\wedge 2}$ for ^{27}Al nuclear spin ($I = 5/2$) and quadrupole frequency, $\nu_Q = 3e^2qQ/[2I(2I-1)h]$; $b = 3K_{\mathrm{ax}}$, where K_{ax} is anisotropic shift. The first term is the broadening from second order quadrupole interactions ($\Delta\nu \sim a/\nu_0$) and the second term is from electric field gradient (EFG) and Knight shift tensor distributions ($\Delta\nu \sim b\nu_0$). The measured results are summarized in Table I. It is worth noting here that any isotropic shift from the fluctuations of Knight shift tensors will be small and can be neglected. The measured ^{27}Al peak shifts are equal to the isotropic shifts by simulating the static spectra with featureless and symmetric lines in SIMPSON [23] (see Fig. 1 and simulation parameters in Table I). This corroborates the argument that the ^{27}Al shifts in the MGs are mainly from the Fermi contact contribution which scales with $g_s(E_f)$.

Quantum mechanical calculations have been carried out in Zr(Cu/Ni)Al-based MGs and compounds, in the interest of achieving essential physics governing the change of electronic density of states on Al sites and its effect on mechanical properties [14,24]. The calculations indicate a strong directional bonding character due to the hybridized Al $3p$ and TM (TM = Zr, Ti, Cu, Ni) d orbitals evidenced by the distribution of the density of states at energy scales, although they are still inevitably metallic. The strong pd hybridization is responsible for weak Al-Al sp hybridization and low Al $3s$ DOS near the Fermi energy. The Al $3s$ states shift to lower binding energy (~ 9 eV) below the Fermi level, close to atomic energy level, in valence bands, indicating Al $3s$ is in nonbonding states and weakly participate in bonding. Theoretical calculations show no significant core level shift in TM-Al alloys and preclude the validity of interatomic charge transfer model in these alloys [25,26]. This indicates that the magnitude of $g_s(E_f)$, manifested as ^{27}Al Knight shifts in this case, reflects the degree of pd hybridization. Gschneidner and *et al.* [19] recently suggests the absence of d-band electrons near the Fermi level accounts for the ductility in intermetallic compounds (B_2 type) and the bonding electrons predominantly being s-like with little or no d-bonds exhibit large ductility. As ductile behavior requires high degree of bond mobility, high degree of s wave function participation in the bonding is a necessary condition for an improved ductility [18]. MGs will be expected to exhibit brittleness if $g_s(E_f)$ yields very small, or ductile if the electronic configuration becomes mostly s like and more likely uniform valence charge density since the bonding will be more nondirectional in this case. The pd hybrid bonds are more prone to be broken for the obvious change of the overlap of atomic orbital during atoms shear moving, while nondirectional s character bonds showing good

TABLE I. Anisotropic shift and quadrupole coupling constant, $C_Q(= e^2qQ/h)$ parameters for two MGs measured in variable magnetic field experiments. Axial symmetry parameters, η^{CS} and η^Q for KSA and EFG tensors are considered to be 0 within SIMPSON simulation.

MGs	Anisotropic shift (ppm)	Isotropic shift (ppm)	e^2qQ/h (MHz)
$Zr_{61}Cu_{17.8}Ni_{12.8}Al_{7.9}Sn_{0.5}$	95 ± 5	360 ± 2	3.73 ± 0.2
$Zr_{61}Cu_{15.8}Ni_{12.8}Al_{7.9}Sn_{2.5}$	85 ± 4	341 ± 2	4.23 ± 0.2

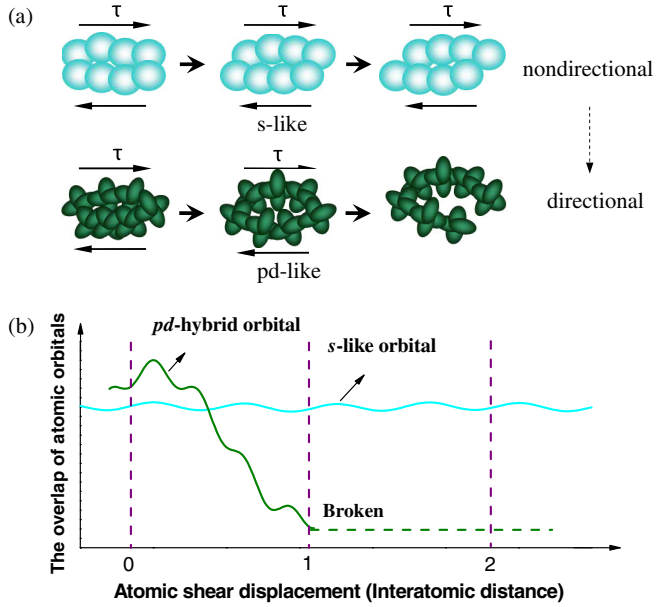

FIG. 3 (color online). (a) A schematic illustration of the overlap of nonpolarizable *s*-like and *pd* hybrid atomic orbitals during shear; (b) the overlap of atomic orbital versus the atomic shear displacement. The overlap of *s*-like atomic orbital remains almost constant during shear; *pd* hybrid atomic orbitals subjected to shear overcome a balance position in which the overlap between bond orbitals reduces to much less than *s*-like orbital since *p*-*d* hybrid orbital extends within one atomic distance, while *s* orbital extends much further with a significant overlap beyond second nearest neighbors.

mobility can absorb more energy at crack tip as atoms can yield long distance, exhibiting more plasticity and dissipating more amount of fracture energy, see the sketch in Fig. 3.

The hybridization between sp solute such as Al (or Si, B, P) p with solvent TM d states has also been experimentally evidenced in various sp element containing alloys and compounds [27,28]. For instance, it has been revealed in electron energy loss spectroscopy by the observation of common states, characteristic white lines (TM L_{2-3} peaks) and the itinerant hybridization model has successfully explained the reduction of magnetic moment at TM site in NiAl and CoAl. Another proof is the observation of Al-TM bond shortening in MGs [29,30]. Furthermore, ^{27}Al shifts from the Fermi contact contribution has been correlated with the hybridization induced reduction of $g_s(E_f)$ in Al-containing compounds [16,31]. Our result of the correlation of ^{27}Al shifts with fracture energy indicates that the addition of Sn strongly perturbs the sp bands and thus affects bond mobility in the MGs. ^{27}Al shifts from the Fermi contact contribution could be used as an order parameter to probe $g_s(E_f)$ and characterize bond mobility of TM-Al bonds in MGs, which is hardly accessible by other techniques.

In summary, we have identified NMR signatures of ductile versus brittle nature of MG materials in the local features of its *s*-character electron DOS in the vicinity of Fermi energy, which is usually inaccessible by other experimental techniques. The nonmonotonic evolution of ^{27}Al NMR isotropic shifts is correlated with BDT induced by microalloying. Our NMR result of strong correlation of NMR shifts with fracture energy strongly supports the electronic origin of microalloying induced embrittlement in alloys and compounds and also reveals the nature of bond mobility mechanism in the MGs.

We thank L. Ma and W. Q. Yu from Renmin University of China for the help of variable magnetic field measurements. This work was supported by the Hundred Talents Program of the Chinese Academy of Sciences, NSF of China (51071171 and 50921091), and the National Basic Research Program of China (MOST 973, grant No. 2010CB731603 and No. 2011CB012806).

*Corresponding author.
xi@iphy.ac.cn

[1] A. Inoue, Acta Mater. **48**, 279 (2000).
[2] C. A. Schuh, T. C. Hufnagel, and U. Ramamurty, Acta Mater. **55**, 4067 (2007).
[3] A. S. Argon, Acta Metall. **27**, 47 (1979).
[4] M. L. Falk and J. S. Langer, Phys. Rev. E **57**, 7192 (1998).
[5] J. D. Bernal and J. Mason, Nature (London) **188**, 910 (1960).
[6] D. B. Miracle, Nature Mater. **3**, 697 (2004).
[7] H. W. Sheng, W. K. Luo, F. M. Alamgir, J. M. Bai, and E. Ma, Nature (London) **439**, 419 (2006).
[8] H. L. Peng, M. Z. Li, and W. H. Wang, Phys. Rev. Lett. **106**, 135503 (2011).
[9] V. Y. Kazimirov, Phys. Rev. B **80**, 214117 (2009).
[10] G. Duscher, M. F. Chisholm, U. Alber, and M. Ruhle, Nature Mater. **3**, 621 (2004).
[11] L. Zhang, Y. Q. Cheng, A. J. Cao, J. Xu, and E. Ma, Acta Mater. **57**, 1154 (2009).
[12] G. Trambly de Laissardière, D. N. Manh, L. Magaud, J. P. Julien, F. Cyrot-Lackmann, and D. Mayou, Phys. Rev. B **52**, 7920 (1995).
[13] C. P. Slichter, *Principles of Magnetic Resonance* (Springer-Verlag, New York, 1996), 3rd ed., p. 113.
[14] X. K. Xi, M. T. Sandor, H. J. Wang, J. Q. Wang, W. H. Wang, and Y. Wu, J. Phys. Condens. Matter **23**, 115501 (2011).
[15] L. H. Chou and T. J. Rowland, Phys. Rev. B **45**, 11580 (1992).
[16] C. S. Lue, B. X. Xie, S. N. Horng, J. H. Su, and J. Y. Lin, Phys. Rev. B **71**, 195104 (2005).
[17] Y. Q. Cheng, E. Ma, and H. W. Sheng, Phys. Rev. Lett. **102**, 245501 (2009).
[18] M. E. Eberhart, R. M. Latanision, and K. H. Johnson, Acta Metall. **33**, 1769 (1985).
[19] K. A. Gschneidner, M. Ji, C. Z. Wang, K. M. Ho, A. M. Russell, Y. Mudryk, A. T. Becker, and J. L. Larson, Acta Mater. **57**, 5876 (2009).
[20] W. L. Johnson and K. Samwer, Phys. Rev. Lett. **95**, 195501 (2005).

[21] See supplemental material at http://link.aps.org/supplemental/10.1103/PhysRevLett.107.236403 for the details of variable field experimental methods.
[22] C. C. Yuan and X. K. Xi, J. Appl. Phys. **109**, 033515 (2011).
[23] M. Bak, J. T. Rasmussen, and N. C. Nielsen, J. Magn. Reson. **147**, 296 (2000). For program and examples see, http://bionmr.chem.au.dk/download/
[24] Q. He, Y. Q. Cheng, E. Ma, and J. Xu, Acta Mater. **59**, 202 (2011).
[25] C. D. Gelatt, A. R. Williams, and V. L. Moruzzi, Phys. Rev. B **27**, 2005 (1983).
[26] P. Ravindran and R. Asokamani, Phys. Rev. B **50**, 668 (1994).
[27] W. Hanke, J. Hafner, and H. Bilz, Phys. Rev. Lett. **37**, 1560 (1976).
[28] G. A. Botton, G. Y. Guo, W. M. Temmerman, and C. J. Humphreys, Phys. Rev. B **54**, 1682 (1996).
[29] A. Sadoc, M. Sabra, O. Proux, J. L. Hazemann, K. S. Bondi, and K. F. Kelton, Philos. Mag. **88**, 2569 (2008).
[30] A. Frenkel, E. A. Stern, A. Voronel, A. Rubshtein, Y. Ben-Ezra, and V. Fleurov, Phys. Rev. B **54**, 884 (1996).
[31] C. S. Lue, T. H. Su, B. X. Xie, and C. Cheng, Phys. Rev. B **74**, 094101 (2006).